JOURNAL OF CATALYSIS 82, 160–170 (1983)

Highly Dispersed Rhodium/Polyphosphine Metal Catalysts: Preparation and Characterization

GIORGIO COCCO, STEFANO ENZO, FRANCESCO PINNA, AND GIORGIO STRUKUL

Facoltà di Chimica Industriale, Università di Venezia, 30123 Venezia, Italy

Received September 9, 1982

The preparation of novel rhodium metal catalysts, dispersed on styrene–2% divinylbenzene copolymer, functionalized with phosphine groups, is reported. The reduction temperature was chosen on the basis of temperature programmed reduction (TPR) experiments. Thermogravimetric analysis (TGA) indicates that the polymeric network in these materials is stable up to 473 K. The physical properties of the metallic phase were determined with X-ray scattering techniques (SAXS and WAXS). These techniques showed that the metal particle size and dispersion were determined mostly by the number of phosphine groups present on the support. This suggested the existence of a strong metal–ligand interaction. This fact was confirmed by an infrared study of CO absorption onto the catalysts. All polyphosphine supported samples showed CO bands which were assigned to polymer-anchored $PRh(CO)_2$ moieties.

INTRODUCTION

The interest in the preparation of supported metal catalysts arises basically from the possibility of obtaining a high dispersion of metal with consequent increase in the surface area, which is the key parameter for their activity and selectivity (*1*).

The obtainable degree of dispersion depends both on the metal–support interactions and on the possibility of reducing the metal precursor under mild experimental conditions (*2*). The former are generally difficult to define, but must be such to prevent further agglomeration of small metallic particles into larger aggregates.

From this point of view the presence on the support of good donor ligands capable of stabilizing zerovalent metal species through strong coordinative interactions should, in principle, lead to high metal dispersions. In fact, a ligand should (i) reduce the coordinative unsaturation of the naked metal atoms, and (ii) prevent, to some extent, the intense migration of metal on the support surface through chemical bonding.

With this in mind, we prepared a series of rhodium metal catalysts supported on styrene–divinylbenzene containing phosphine groups. These ligands offer the advantage of a strong and easily definable metal–support interaction and allow a facile correlation between the density of the attached functional groups and the metal crystallite sizes. Moreover, to minimize sintering effects during the preparation and activation of the catalysts (*3*), we chose, as precursor, an easily accessible organometallic complex $[Rh(COD)Cl]_2$ (COD = 1,5-cyclooctadiene), which could be reduced with hydrogen at a relatively low temperature. In recent years the use of thermally labile precursors has received increasing interest and has been performed mainly with two different classes of compounds: (i) purely organometallic species (*4*), and (ii) metal carbonyl cluster compounds (*5*), the advantages and limitations of which have been extensively studied and reviewed.

In this paper we report a study of the influence of the number of phosphine groups on the dimensions of Rh metal particles determined by X-ray scattering techniques, in particular Small Angle X-ray Scattering (SAXS) and Wide Angle X-ray Scattering (WAXS). The characterization of the catalysts also includes infrared spectroscopy (IR), thermogravimetric analysis

0021/9517/83 $3.00

(TGA) and temperature programmed reduction (TPR).

In the second part of this study we shall consider how the presence of the phosphine ligands influences the reactivity of these catalysts.

EXPERIMENTAL

Supports

Two different kinds of support were used: Fluka styrene–2% divinylbenzene copolymer (beads, 200–400 mesh) and polyphosphines. The preparation of polyphosphine supports (PolyPPh$_2$) involved the addition of THF solutions of LiPPh$_2$ to Merrifield Polymer Fluka (chloromethylated styrene–2% divinylbenzene copolymers available with various chlorine contents, beads, 200–400 mesh) according to the method of Relles and Schluenz (*6*).

All operations were carried out under nitrogen atmosphere. The various samples, once dried, were stored in air at room temperature.

Catalysts

Appropriate amounts of support and [Rh(COD)Cl]$_2$, prepared according to Chatt and Venanzi (*7*), were placed solid in a round-bottomed flask and evacuated for 15 min. N_2 saturated CH_2Cl_2 was added under nitrogen and the mixture vigorously stirred for 15 min. Slow evaporation of the solvent was carried out in a rotary evaporator under slight vacuum to give a deep yellow solid. The beads were dried in vacuo (10^{-2} Torr; 1 Torr = 133,3 N m^{-2}) at room temperature overnight.

Catalysts were reduced in flowing hydrogen (9 liter/h) while heating at 5 K per min to 403 K with a 18-h hold at that temperature. Samples were cooled down to room temperature in hydrogen and stored under nitrogen.

The same procedure was employed for the preparation of the reported Rh/SiO_2 (Akzochemie F22) catalysts.

TABLE 1

Analytical Data of the Catalysts

Catalyst	P(%)	Rh(%)
Rh-1(PolyPPh$_2$)[a]	1.6	1.0
Rh-2(PolyPPh$_2$)	6.2	9.9
Rh-3(PolyPPh$_2$)	1.7	0.6
Rh-4(PolyPPh$_2$)	1.7	1.6
Rh-5(PolyPPh$_2$)	1.2	0.5
Rh-6(PolyPPh$_2$)	1.2	1.0
Rh-7(PolyPPh$_2$)	1.2	2.0
Rh-8(PolyPPh$_2$)	1.2	5.0
Rh-9(PolyPPh$_2$)	1.7	3.0
Rh-10(PolyPPh$_2$)	0.5	0.5
Rh-11(PolyPPh$_2$)	0.5	1.0
Rh-12(PolyPPh$_2$)	0.5	2.0
Rh-13(PolyPPh$_2$)	0.5	5.0
Rh-14(Poly)[b]	—	1.1
Rh-15(Poly)	—	6.8
Rh-16(SiO_2)	—	2.0

[a] PolyPPh$_2$ = Phosphinated styrene–2% divinylbenzene copolymer.

[b] Poly = Styrene–2% divinylbenzene copolymer.

Microanalyses for Rh and P contents were performed by Analytisches Laboratorium, Elbach-West Germany.

Analytical data are reported in Table 1.

Thermogravimetric analysis (TGA)

This was performed on a Netzsch 429 STA instrument under N_2 flow. Samples (100 mg) were previously evacuated at 10^{-2} Torr at 343 K for 10 hr. The heating rate from 298 K to 673 K was 5 K/min.

Temperature Programmed Reduction (TPR)

Principles and apparatus of TPR method have already been described (*8*). The reducing gas (5% H_2 in Ar) was purified over an Oxy-trap (Alltech), dried in a molecular sieves trap cooled at 195 K and introduced at a 40-ml/min rate into a 50–100 mg sample. The heating rate was 5 K/min.

SAXS procedure

SAXS measurements were carried out with a Kratky camera aligned to obtain the

condition of "infinite primary beam" and equipped with an electronic step scanner. Ni filtered Cu$K\alpha$ radiation with a pulse height discriminator and a proportional counter were employed. Owing to the favorable system under investigation, no masking liquids were required to obtain meaningful SAXS data. A preset count mode was employed; several runs were taken to accumulate 10^{-5} counts per point and the intensities through the passes were averaged. The curve of the support was simply subtracted to that of the catalysts. It is known that the specific surface can be derived from the asymptotic value in the tails of small angle absolute intensities according to (*9*)

$$S_{sp} = \frac{\lim_{h\to\infty} h^3 J(h)}{\pi^2(\Delta\rho)^2 I_e(h)]}$$

where $h = 4\pi \sin\theta/\lambda$ (with 2θ scattering angle and λ = X-ray wavelength) is the scattering vector; $J(h)$ is the slit smeared intensity; $\Delta\rho = \rho_1 - \rho_0$ is the electron density difference between heterogeneities and matrix, and $I_e(h)$ is the scattering intensity of a single electron in the same experimental conditions. To obtain particle size distribution functions from SAXS data it is necessary to introduce some approximations. In the case of infinite dilution and absence of multiple scattering and when the shape is known and is the same for all heterogeneities, the following equation holds for desmeared intensities (*10*):

$$I(h) = (\Delta\rho)^2 \int_0^\infty d_v(R) R^{-\alpha} V^2(R) i_0(hR) dR$$

where α is a dimensional parameter ($\alpha = 2$ for bidimensional heterogeneities, 3 for the three-dimensional case); $d_v(R)$ is the distribution function that states the volume of all particles defined by the size parameter R (e.g., in the case of a sphere, R could be the diameter); $i_0(hR)$ is the intensity scattered by a single particle with size parameter R and volume $V(R)$.

When the shape factor of the particle can be expressed as a square of a Bessel function of the first kind, the volume distribution function can also be obtained analytically by making use of the Titchmarch transform of the scattered smeared intensity (*11*). The final relation for spherical particles stands:

$$d_v(R) \propto R \int_0^\infty [h^3 J(h) - K] \left[2J_0(hR) + J_1(hR)\left(hR - \frac{3}{hR}\right)\right] dh$$

where $K = \lim_{h\to\infty} h^3 J(h)$ is the Porod asymptotic value, J_0 and J_1 are, respectively, first kind Bessel functions of zero and first orders.

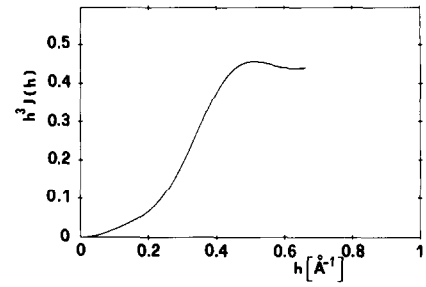

FIG. 1. Porod plot for Rh-1. A constant background has been subtracted from the original intensity data.

The Porod constant was always determined with sufficient accuracy, as illustrated in Fig. 1, so that in the solution function $d_v(R)$ termination effects are negligible (*12*).

From the size distribution it is possible to gain a number of integral parameters representative of the systems under study. Provided that the distribution functions $d(R)$ are normalized, so that

$$\int d(R) dR = 1$$

one can, for example, define a surface weighed mean as

$$D_s = \int_0^\infty R d_s(R) dR$$

or, analogously, a volume weighed mean

$$D_v = \int_0^\infty R d_v(R) dR.$$

Note that $d_v(R)$ and $d_s(R)$ are related as follows:

$$d_v(R) \propto R d_s(R).$$

The percentage exposed $p_{exp}{}^s$, defined as the ratio of the number of surface atoms to the number of total atoms, can be calculated assuming a spherical shape of the particles

$$p_{exp}{}^s = \int_0^\infty \frac{R^3 - (R - 4d_0)^3}{R^3} d_v(R) dR$$

where d_0 is the atomic diameter of rhodium (bilayer approximation).

WAXS Procedure

The samples were observed with a vertical Philips powder diffractometer connected to a highly stabilized generator with an X-ray tube working at 2 kW. Ni filtered Cu$K\alpha$ radiation, Soller slits, a graphite focusing crystal as a monochromator, and a scintillation counter supplied with a pulse analyzer were employed.

A Fourier analysis (*13*) of the peak profile was applied for the samples having reflections with a strong enough intensity.

Suitable angular ranges were scanned step by step through various Rh line profiles, provided that 40,000 counts per point were accumulated. The background was removed by subtracting the scattering of the support material independently recorded in the same experimental conditions of the catalysts.

The deconvolution from instrumental and spectral effects was done for convenience in the Fourier domain, according to Stokes' method (*14*). The resultant coefficients $A(L)$, where $L = nd_{hkl}$ is a distance normal to the reflecting (hkl) planes, are the product of a particle size coefficient $A^p(L)$ and a microstrain coefficient $A^e(L)$. The crystallite size distribution may be extracted from $A(L)$ when a multiple order series is experimentally available, since

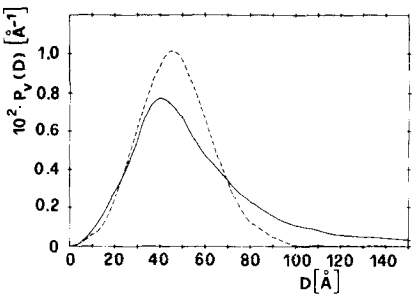

FIG. 2. Crystallite size distribution functions for Rh-14 from Fourier analysis of (111) (solid line) and (200) (dashed line) peak profiles.

$A^e(L)$ depends on interplanar distance, while $A^p(L)$ does not (*15*). A single line analysis technique may be used alternatively (*16*). From the initial slope of the $A^p(L)$ vs L curve an average particle size (surface weighed) is determined (*13*). These data may be further analyzed to obtain the volume crystallite size distribution $p_v(D)$ (*17*) according to

$$p_v(D) = D \left[\frac{d^2 A^p(L)}{dL^2}\right]_{L=D}$$

From this size distribution one can again recover averaged values such as surface means, volume means, percentage exposed, and specific surface. The approximations needed for these calculations are essentially the same as used in the SAXS analysis: we generally assume to deal with nearly spherical particles. Physically, this is justified as far as WAXS diagrams show peaks leading to similarly ranged size distributions, independently of the observed (hkl) planes. In Fig. 2 we report the crystallite size distribution for the sample rhodium-14 computed starting from the (111) and (200) line profiles according to the procedure just described.

Infrared Spectroscopy (IR)

Samples previously ground in a ball mill were left under research grade CO flow (5 liter/h) at 348 K for 4 h. They were cooled down under CO and discharged; infrared spectra in the region of 1500–2500 cm^{-1}

were recorded in nujol mull on a Perkin–Elmer 683 instrument.

RESULTS AND DISCUSSION

The reaction of $[Rh(COD)Cl]_2$ with free tertiary phosphines is well known (*7*) and leads to the formation of bridge-splitting Rh(COD)(P)Cl-type complexes (P = tertiary phosphine). The same kind of process can be envisaged in our system (reaction (1)).

$$\text{PolyPPh}_2 + [Rh(COD)Cl]_2 \rightarrow (\text{PolyPPh}_2)Rh(COD)Cl \quad (1)$$

PolyPPh_2 = polymeric phosphine

On the other hand, excess of phosphine with respect to rhodium is known to give rise, in solution, to equilibrium mixtures also containing $[Rh(COD)P_2]Cl$ complexes (*18, 19*). Although in the polymeric system the ratio between the number of phosphine groups and rhodium introduced is over $\frac{1}{1}$ in most cases, the presence of significant amounts of this type of compounds can be neglected because of the following considerations: (i) the extent of the above equilibrium in solution is generally small, especially with PPh_3 (*19*), and (ii) the availability of phosphine groups in proximity of an already anchored metal is certainly lower than the theoretical P/Rh ratio because of the limited mobility of a polymeric phosphine with respect to the same ligand in solution. Further experimental support derives from previous unsuccessful attempts to prepare polymeric $[(\text{PolyPPh}_2)_2Rh(NBD)]^+$ complexes (NBD = 2,5-norbornadiene) starting from PolyPPh_2 and $[Rh(NBD)Cl]_2$ (*20*).

Hence our system can be envisaged, before reduction to metal, as constituted from polymer-anchored $(\text{PolyPPh}_2)Rh(COD)Cl$, physisorbed $[Rh(COD)Cl]_2$, and some free phosphine groups. Catalysts Rh-14 and Rh-15, prepared according to the same experimental procedure but using as support styrene–2% divinylbenzene copolymer, will contain only physisorbed $[Rh(COD)Cl]_2$.

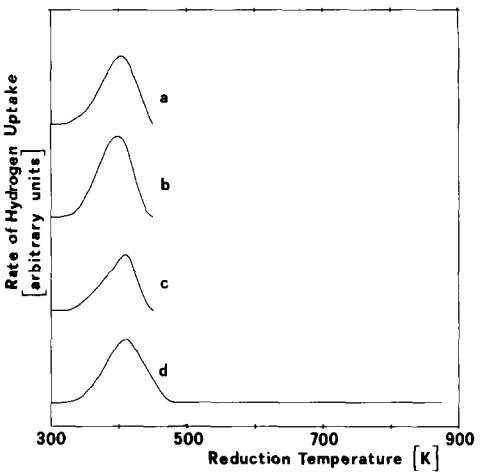

FIG. 3. Temperature-programmed reduction curves: (a) Rh-8; (b) Rh-15; (c) Rh-8 after Sohxlet extraction; (d) Rh/Silica.

All catalysts were reduced in flowing hydrogen heating from room temperature up to 408 K at a rate of 5 K/min and then maintaining the temperature constant overnight. The temperature was chosen on the basis of some TPR experiments. They were performed to determine the temperature at which the maximum rate of decomposition occurs. A typical experiment is reported in Fig. 3,a for Rh-8. All samples were heated from room temperature up to 453 K at a rate of 5 K/min. As shown, only one reduction profile ranging between 323 and 448 K with a maximum centered at 403 K can be detected, despite the presence of two different precursors to the metallic species. As a matter of fact, TPR experiments, carried out on Rh-15 (Fig. 3,b) containing only physisorbed $[Rh(COD)Cl]_2$ as precursor and on a catalyst containing only polymer-anchored $(\text{PolyPPh}_2)Rh(COD)Cl$ species (Fig. 3,c), show maxima at 398 K and 408 K, respectively. The latter catalyst was prepared from Rh-8 after extraction of the physisorbed $[Rh(COD)Cl]_2$ in a Sohxlet apparatus with CH_2Cl_2 for 30 h under N_2. TPR investigation above 453 K is prevented because of problems of thermal stability. To

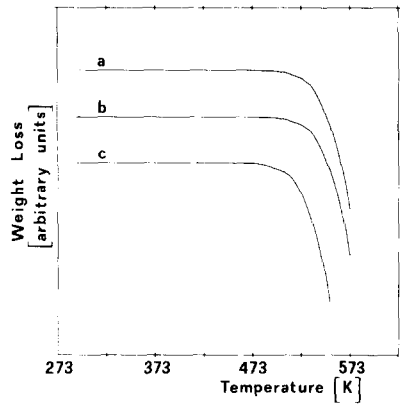

FIG. 4. Thermogravimetric curves: (a) polyphosphine support (P 1.7%); (b) styrene–2% divinylbenzene copolymer; (3) Rh-9.

make sure that no other reduction steps were present above this temperature, a further TPR experiment was carried out on a $[Rh(COD)Cl]_2/SiO_2$ sample prepared according to the general method described. As it appears from Fig. 3,d, only a single reduction profile, with maximum at 408 K, can be detected, even heating up to 873 K.

All these data prove umambiguously that under the experimental conditions used for the preparation of the catalysts all the precursor is homogeneously and completely reduced to the metallic species.

When dealing with catalysts where organic polymers are used as supports, their relatively low thermal stability is one of the problems that must be considered. Our catalysts were therefore studied with TGA to determine the temperature range in which they could be used without destroying the polymeric network of the support. All samples were analyzed under N_2 flow to avoid surface contamination due to the presence of oxygen. They were previously evacuated overnight at 343 K and 10^{-2} Torr.

All polyphosphines used as support (P content varying between 0.5 and 6.2%) are thermally stable up to 493 K (in Fig. 4,a a typical example is reported). Above this temperature, a severe weight loss is recorded, which can be ascribed to a collapse of the polymeric matrix. Identical results are obtained using styrene–2% divinylbenzene copolymer (Fig. 4,b). With the Rh catalysts under the same experimental conditions the decomposition temperature is about 20 K lower, independent of the metal content of the individual catalysts (Fig. 4,c). Since a loss of Rh metal is unrealistic at these temperatures, the weight loss might be again ascribed to a decomposition of the matrix.

The atomic structure and the morphological parameters of rhodium catalysts after reduction were determined by using the X-ray scattering techniques SAXS and WAXS, each of them having its proper advantages and limitations.

The present styrene–divinylbenzene supported rhodium catalysts are particularly suited for SAXS analysis. In fact, they present a high electron density difference between metal phase and support material. Moreover, the texture of the supports does not give rise to interference effects with the metal scatterers (*21*). Under these circumstances it was also possible to collect satisfactory data for the more diluted samples.

The results obtained by a combination of these techniques are summarized in Table 2. The consistency between the average values from SAXS and WAXS turned out

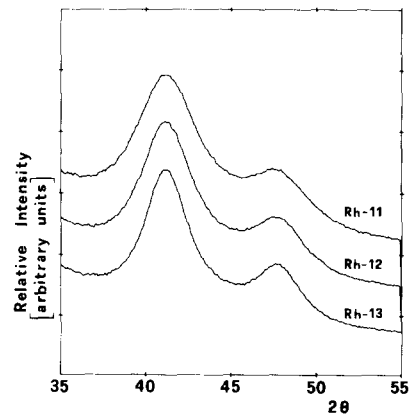

FIG. 5. WAXS diagrams showing narrowing of Rh(111) and (200) peak profiles for three samples on increasing metal loading. A progressive overlapping of the (200) line with the tail of (111) peak is evident.

TABLE 2

Main Parameters Obtained from Catalyst Characterization

Catalyst	Particle size (Å)[a]		Surface Area (m^2/g)		Percentage exposed[b]		P/Rh_t	P/Rh_s
	D_s	D_s^w	SAXS	WAXS	P_{exp}^s	P_{exp}^w		
Rh-1	15	—[c]	322	—[c]	0.90	—[c]	5.3	5.8
Rh-2	15	—[c]	322	—[c]	0.93	—[c]	2.1	2.3
Rh-3	17	—[c]	293	—[c]	0.88	—[c]	9.4	10.7
Rh-4	19	—[c]	260	—[c]	0.82	—[c]	3.5	4.3
Rh-5	12	—[c]	370	—[c]	0.95	—[c]	8.0	8.4
Rh-6	16	—[c]	335	—[c]	0.89	—[c]	4.0	4.5
Rh-7	18	—[c]	263	—[c]	0.87	—[c]	2.0	2.3
Rh-8	29	27	166	149	0.66	0.61	0.8	1.2
Rh-9	19	—[c]	251	—[c]	0.81	—[c]	1.9	2.3
Rh-10	26	24	187	168	0.71	0.64	3.3	4.6
Rh-11	29	27	167	150	0.68	0.61	1.7	2.4
Rh-12	44	42	111	100	0.53	0.48	0.8	1.6
Rh-13	67	65	72	65	0.35	0.32	0.3	0.9
Rh-14	48	42	101	115	0.49	0.53	—	—
Rh-15	83	97	58	50	0.30	0.27	—	—
Rh-16	20	—[c]	250	—[c]	0.82	—[c]	—	—

[a] D_s represents the surface weighed diameter computed from SAXS size distribution, while the analogous from WAXS distribution function is denoted by D_s^w.

[b] Defined as the ratio between the number of Rh surface atoms and the total number of metal atoms. P_{exp}^s computed from SAXS; P_{exp}^w computed from WAXS size distribution function.

[c] Not detectable.

satisfactorily and suggested that the particles had a well-defined crystalline arrangement (*22*). The percentage of samples exposed varied from 30 to 95% approximately. Increased metal loading for a series of catalysts containing P 0.5% resulted in a narrowing of the WAXS (111) peak profiles and in a shift of the SAXS size distributions towards large dimensions, as reported in Figs. 5 and 6, respectively.

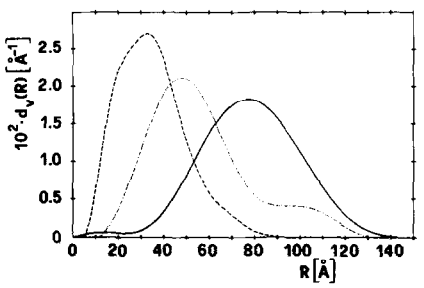

FIG. 6. SAXS volume distribution functions, for a series of three samples on increasing metal loading: Rh-11 (dashed); Rh-12 (dotted); Rh-13 (solid).

To exploit the effect of P content on dispersion we prepared a sample with high loading of both P and Rh (Rh-2), according to the procedure illustrated. The SAXS size distribution function for this sample is presented in Fig. 7. These data agree indirectly with the relevant wide angle diffractogram reported in this figure. Taking into account the fact that the metal phase is highly concentrated and that a complete reduction by hydrogen was checked by TPR, the absence of a discernible X-ray peak in the angular range correspondent to the more intense (111) line for the crystalline rhodium confirmed that the particles were very small. This behavior was completely different in the case of the Rh-15 sample, which had a high Rh loading and was prepared starting from a polymeric support without

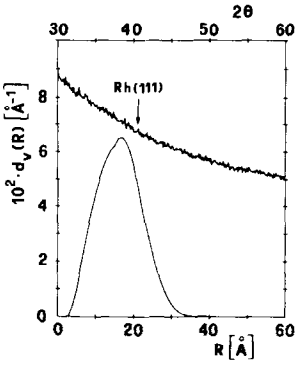

FIG. 7. SAXS volume distribution function and WAXS diagrams for Rh-2. Notice the absence of Rh (111) line profile at 41.10°.

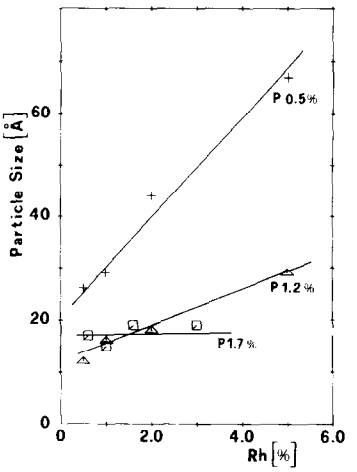

FIG. 9. Correlation between metal particle size and rhodium content for three series of catalysts.

P. Its SAXS and WAXS size distribution functions are reported in Fig. 8.

Owing to the presence of two different precursors (polymer-anchored (PolyPPh$_2$) Rh(COD)Cl] and physisorbed [Rh(COD) Cl$_2$), a bimodal distribution of particle size might be suspected. However, all the observed distribution patterns exclude this possibility, indirectly support the previous TPR experiments, and confirm that a homogeneous growth of metal particles took place.

In getting the size distribution function from the SAXS data, the shape of the particles must be known a priori. Assuming a spherical shape of rhodium particles might be questionable in view of the findings by Yates *et al.* (*23*), who reported experimental evidence suggesting that rhodium catalysts dispersed on alumina with percentage exposed near 100% have a raftlike structure. On the other hand, a raftlike structure has been found to be quite incidental. Moreover, other authors have questioned its being a realistic model for the rhodium particle structure both on silica (*24*) and on alumina (*25*). We tried to compute the particle size distribution function by imposing the shape factor for rafts using Vonk's procedure (*26*). However, we found that the curve reconstructed from the final size distribution fit the original intensity better data when assuming a spherical shape factor for heterogeneities.

A correlation among the P and Rh contents and the metal particle sizes derived from SAXS is reported in Fig. 9. As it appears, when the P percentage is sufficiently low (0.5% or 1.2%), an increasing trend is evident for the particle diameter as the Rh content increases, although in the 0.5% case this effect is more marked. Conversely, the particle diameter for P 1.7% remains practically unchanged in the range of metal content considered. These results strongly support the hypothesis that the obtainable metal dispersion is mostly determined by the phosphorus content. This is more evident in Fig. 10, where the metal particle diameter is correlated to the P% for

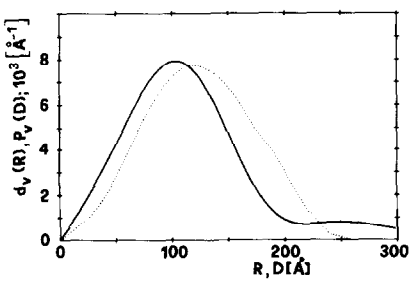

FIG. 8. WAXS (solid) and SAXS (dotted) size distribution functions for Rh-15.

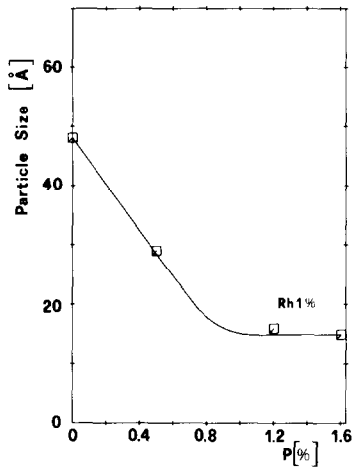

FIG. 10. Relationship between metal particle size and phosphorus content for catalysts with the same metal loading.

a series of catalysts with constant Rh content (1%).

Phosphine ligands are known to stabilize group VIII transition metals in their lower oxidation states, so, when zerovalent Rh atoms are initially produced upon reduction, we can still envisage a sort of bonding interaction between the "naked" metal atoms and the phosphine groups. This interaction on the one hand reduces the coordinative unsaturation and on the other hand inhibits to some extent the free migration of metal atoms to coalesce into large particles.

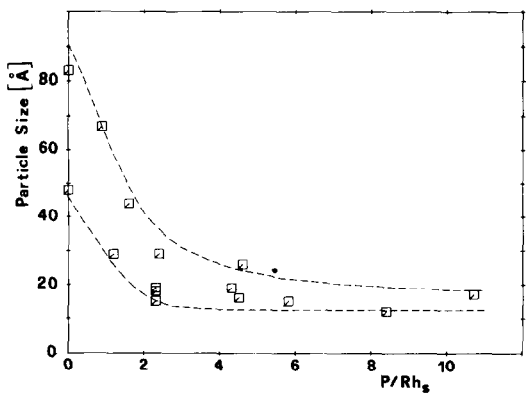

FIG. 11. Relationship between metal particle size and phosphorus/rhodium (surface) ratio for all catalysts.

In the generation of metal aggregates, the ratio between the total number of phosphines and the surface Rh atoms tends to increase as the size grows, with consequent stabilization due also to the high mobility of the organic polymeric support (*27*). As a limit situation the metal particle could be envisaged as surrounded by a "cage" of phosphines. As a matter of fact, it is significant that, if the starting P/Rh(total) ratio is converted into the final P/Rh(surface) ratio (Table 2), the values obtained are largely over unity in all cases but one. Once this topological situation has been achieved, a further addition of phosphines will have no influence on the metal particle dimensions. This is particularly evident in Fig. 10 for a constant amount of metal, but, significantly, the same correlation appears also in Fig. 11, where all the catalysts have been plotted in terms of their P/Rh(surface) ratio, independently of the individual P and Rh absolute amounts.

The experimental data reported so far have pointed out the relationship between the obtainable metal particle size and the number of phosphine groups present on the support. However, these results constitute only indirect evidence for a strong metal support interaction through phosphine groups. Therefore, to get a better understanding and more direct evidence, an infrared study of CO absorption onto these catalysts was undertaken. All catalysts supported on polyphosphines showed CO bands at 2075 and 1998 cm^{-1} (Fig. 12,a,b). Such bands are not typical of rhodium crystallites supported on, for example, silica (*28*) or alumina (*23*), but resemble those reported by Gates *et al.* (*29*) (2078, 2008) and Iwatate *et al.* (*30*) (2080, 2000, 1856) for closely related systems. The materials reported by both these authors involved ligand exchange of $Rh_6(CO)_{16}$ with phosphinated styrene–divinylbenzene copolymers, followed by carbon monoxide treatment to restore the coordinated CO ligands that were lost during the preparation. The infrared bands observed have been at-

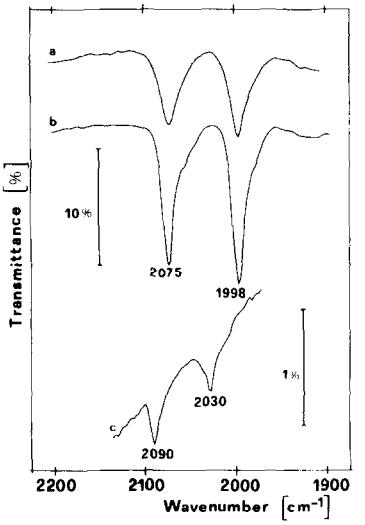

FIG. 12. Metal carbonyl infrared spectra of polymer supported catalysts: (a) Rh-11; (b) Rh-6. Notice the increase of the band intensity on increasing surface area; (c) Rh-15.

tributed to polymer-anchored $Rh_6(CO)_{16-n}P_n$ molecular clusters by Iwatate *et al.* (*30*), who suggested that during the preparation procedure the Rh_6 core remained intact. The fact that we observed practically identical bands on our metallic catalysts can be taken as direct evidence for a coordinative interaction between the phosphine ligands and the metal surface. The two carbonyl bands can be assigned to the symmetric (2075 cm^{-1}) and antisymmetric (1998 cm^{-1}) stretching vibrations of a $PRh(CO)_2$ moiety in analogy to the conclusions of Thornton *et al.* (*31*) and Knötzinger *et al.* (*32*) for samples prepared by attachment of $Rh_6(CO)_{16}$ onto phosphine modified silica. However, it has to be pointed out that the formation of the $PRh(CO)_2$ entities take place at the surface of the metal particles, since we observed an increase in the intensity of the carbonyl bands as the specific surface of the metal increased (Fig. 12,a,b). A more convincing argument for the existence of phosphine–rhodium interactions can be gained by the observation of the carbonyl spectra of Rh-14 and Rh-15 (which do not contain phosphine groups), where only very weak bands at 2090 and 2030 cm^{-1} can be detected (Fig. 12,c). Such bands are typical (*28*) of the symmetric and antisymmetric stretching modes for CO adsorbed on the edges of polycrystalline Rh. Somewhat surprisingly, we were never able to detect the band at about 2045 cm^{-1}, characteristic (*28*) of CO adsorbed on Rh crystal faces, despite the fact that, in many cases, the presence of crystalline rhodium was directly detected with WAXS. In this respect our catalysts differ from those reported by Gates *et al.* (*29*), although the infrared data reported by these authors refer to the same polymers in the form of membranes instead of beads, as in the present case. Alternatively, since different experimental procedures were employed in recording the infrared spectra, we must consider also the possibility that the band at 2045 cm^{-1} might be lost because of desorption during workup for IR analysis.

In conclusion, the initial hypothesis of utilizing very strong metal–ligand interactions to prepare very dispersed metal catalysts has proved correct; moreover, this approach may lead to a control of the metal particle size through appropriate dosing of the ligand concentration. This kind of preparative technique has potentially wide implications since it can be applied to a variety of metals due to the fact that many organic polymers and some inorganic oxides can be easily functionalized with a wide variety of ligands (*33*). However, the impact of the presence of coordination ligands on the catalytic properties of these catalysts remains to be considered and will be the subject of the following paper.

ACKNOWLEDGMENT

The financial support from C.N.R. (Roma) is gratefully acknowledged.

REFERENCES

1. Anderson, J. R., "Structure of Metallic Catalysts." Academic Press, New York, 1975.
2. Moss, R. L., Anderson, R. B., and Dewson, P. T., Eds., "Experimental Methods in Catalytic Re-

search," Vol. III. Academic Press, New York, 1976.
3. Wanke, S. E., and Flynn, P. C., *Catal. Rev. Sci. Eng.* **12,** 93 (1975).
4. Yermakov, Yu. I., *Catal. Rev. Sci. Eng.* **13,** 77 (1976); Yermakov, Yu. I., *J. Mol. Catal.* **9,** 13 (1980) and references therein.
5. Smith, A. K., and Basset, J. M., *J. Mol. Catal.* **2,** 229 (1977); Gates, B. C., and Lieto, J., *Chem. Tech.* **10,** 95 (1980); **10,** 248 (1980) and references therein.
6. Relles, H. M., and Schluenz, R. W., *J. Amer. Chem. Soc.* **96,** 6469 (1974).
7. Chatt, J., and Venanzi, L. M., *J. Chem. Soc.* 4735 (1957).
8. Robertson, S. D., McNicol, B. D., de Baas, J. H., Kloet, S. C., and Jenkins, J. W., *J. Catal.* **37,** 424 (1975).
9. Porod, G., *Kolloid. Z.* **124,** 83 (1951); **125,** 109 (1952).
10. Guinier, A., and Fournet, G., "Small Angle X-ray Scattering." Wiley, New York, 1955.
11. Fedorova, I. S., and Schmidt, P. W., *J. Appl. Cryst.* **11,** 405 (1978).
12. Glatter, O., *J. Appl. Cryst.* **13,** 7 (1980).
13. Warren, B. E., "X-ray diffraction." Addison–Wesley, Reading, Mass., 1969.
14. Stokes, A. R., *Proc. Phys. Soc.* **61,** 382 (1948).
15. Warren, B. E., and Averbach, B. L., *J. Appl. Phys.* **23,** 497 (1952).
16. Ganesan, P., Kuo, H. K., Saavedra, A., and De Angelis, R. J., *J. Catal.* **52,** 310 (1978).
17. Bertaut, E. F., *Acta Cryst.* **3,** 14 (1950).
18. Shapley, J. R., Schrock, R. R., and Osborn, J. A., *J. Amer. Chem. Soc.* **91,** 2816 (1969).
19. Schrock, R. R., and Osborn, J. A., *J. Amer. Chem. Soc.* **93,** 2397 (1971).
20. Strukul, G., Bonivento, M., Graziani, M., Cernia, E., and Palladino, N., *Inorg. Chim. Acta* **12,** 15 (1975).
21. Whyte, T. E., Kirklin, P. W., Gould, R. W., Heinemann, H., *J. Catal.* **25,** 407 (1972).
22. Benedetti, A., Cocco, G., Enzo, S., Piccaluga, G., Schiffini, L., *J. Chim. Phys.* **78,** 961 (1981).
23. Yates, D. J. C., Murrell, L. L., and Prestridge, E. B., *J. Catal.* **57,** 41 (1979).
24. Yacaman, M. J., Romeu, D., Fuentes, S., Dominguez, J. M., *J. Chim. Phys.* **78,** 861 (1981).
25. Fuentes, S., Figueras, F., *J. Catal.* **61,** 443 (1980).
26. Vonk, C. G., *J. Appl. Cryst.* **9,** 433 (1976).
27. Davidova, S. L., and Plate, N. A., *Coord. Chem. Rev.* **16,** 195 (1975).
28. Yang, A. C., and Garland, C. W., *J. Phys. Chem.* **61,** 1504 (1957); Rouco, A. J., and Haller, G. L., *J. Chim. Phys.* **78,** 971 (1981).
29. Jarrell, M. S., and Gates, B. C., *J. Catal.* **54,** 81 (1978); Jarrell, M. S., Gates, B. C., and Nicholson, E. D., *J. Amer. Chem. Soc.* **100,** 5727 (1978).
30. Iwatate, K., Dasgupta, S. R., Schneider, R. L., Smith, G. C., and Watters, K. L., *Inorg. Chim. Acta* **15,** 191 (1975).
31. Thornton, E. W., Knötzinger, H., Tesche, B., Rafalko, J. J., and Gates, B. C., *J. Catal.* **62,** 117 (1980).
32. Knötzinger, H., Thornton, E. W., and Wolf, M., *J. Chem. Soc. Faraday I* **75,** 1888 (1979).
33. Bailey, D. C., and Langer, S. H., *Chem. Rev.* **81,** 109 (1981); Akelah, A., and Sherrington, D. C., *Chem. Rev.* **81,** 557 (1981).